University of Thi-Qar Journal

ISSN (print): 2706- 6908, ISSN (online): 2706-6894

Vol.19 No.1 Agu. 2024

Improvement of Surface Properties of Structural Steel Using (Fe+Ti64+Gray Cast Iron) As TIG Cladding Layer.

Dheyaa F. Kadhim [1,*], Falih H. Saddam [2], Kamaal Sahib M. Al-hamdani [3]

[1] Department of Studying and Planning, University of Thi-Qar, Nasiriyah, Iraq.
Dheyaa.kadhim@utq.edu.iq
[2] Department of Mechanical Engineering, University of Thi-Qar, Nasiriyah, Iraq.
Alazzawi.eng1973@gmail.com
[3] Department of Mechanical Engineering, University of Thi-Qar, Nasiriyah, Iraq.
Kamal-s@utq.edu.iq

https://doi.org/10.32792/utq/utj/vol19/1/3

ABSTRACT

This paper presents a practical study of a mixture of cast iron, Ti-6Al-4V alloy turning flakes, and pure iron powder as a hard coating layer to improve the surface properties of structural steel. A TIG welding machine was used as the heat source to deposit the cladding metal onto the substrate surface. The process parameters for the cladding process were (100 A) and (9, 10, 11 L/min), representing the current and gas flow rate, respectively. Optical microscope, X-ray diffractometer, Vickers hardness test, and Pin on disc tribometer used to investigate the microstructure, phase composition, microhardness, and wear resistance. The results show that the cladding layers consist of FCC and BCC phases, with a small amount of other unknown phases. They also show that samples prepared under a wide range of gas flow rates have a high hardness, approximately two times that of the substrate. wear test results show that the wear rates of samples prepared under a high range of gas flow rates were 1.5 times less than the substrate.

Keywords: Structural steel, Ti6Al4V, TIG Cladding ,Wear rate.

University of Thi-Qar Journal

ISSN (print): 2706- 6908, ISSN (online): 2706-6894

Vol.19 No.1 Agu. 2024

1. INTRODUCTION

Many engineering applications' inefficiency is thought to be mostly caused by wear-related disintegration of present-day machine components. Since the condition of a material's surface layers affects its wear qualities. It has been hypothesized that surface treatment is one way to prevent the failure of contemporary machine components [1-3]. Various hard protective coating materials are being utilized by industrial engineers to improve the surface qualities. Surface alloying is a prevalent method to boost the surface hardness, wear resistance, and durability against corrosion of various materials, including titanium alloys. It forms a hard protective coating using an iron-based alloy. Iron-based alloy coatings have been used for many years on tools, dies, and engineering components because of their exceptional qualities, which include great wear resistance, superior wettability, and high hardness [4]. Several approaches have been used in recent decades to formulate a hard coating layer, such as pack cementation [5] ion implantation [6], PVD [7], and laser beam surface processing [8]. Laser beam processing has made it possible to modify the surface composition and structure to sustain high wear resistance by surface alloying with high energy densities. S. Jiguo et al. prepared the surface containing Ni-Al intermetallics by preplacing Ni and aluminum powder on a Q235 steel plate using a TIG arc source. The intermetallic beads were created using various current levels and surfacing speeds. The phase of α-Fe is generated when elevated current of 121 A and 1.6 mm/s are combined. The formation of the considerable amount of Ni-Al in the γ-(Fe, Ni) inter-granular phase occurs at a current of 81 A and a speed of 0.87 mm/s [9]. S. Islak et al. filled 4 mm radius and 1.5 mm profound cavities substrate with a mixture of FeW and B4C particles in varying particle ratios (10%, 20%, and 40% of B4C in FeW/B4C

University of Thi-Qar Journal

ISSN (print): 2706- 6908, ISSN (online): 2706-6894

Vol.19 No.1 Agu. 2024

mixture). The surface composite was created on the steel substrate using a TIG arc source. On the steel surface, a coating thickness of 2000–2400µm was created. The composite's micro-hardness was four to five times more than that of the foundation material. The highest hardness value of 1095Hv was attained when the mixture contained 40% B4C powder. About 225Hv was the hardness of the basic material. The development of carbide Fe3(C, B) and borides Fe23 (C, B) in the microstructure was the cause of the surface coating's increased hardness[10]. Using organic binders, Cooke et al. combined 53% titanium powder with 47% aluminum powder. The mixture was then preplaced on a pure titanium substrate, maintaining a surface thickness of 0.6 to 1 mm. The powder was melted to form an intermetallic coating on the substrate using a TIG operating at 51 to 101A and at various rates of 2, 3, and 4 mm/s. Glazing at 100A TIG arc current and 2 mm/s resulted in a maximum melt depth of 2 mm. The primary cause of the alloyed layer's creation at a deeper depth is the torch's energy density. The XRD peaks demonstrated that TiAl structure was formed by 60A TIG arc while Ti3Al and TiAl structure was produced by elevated energy of 110A TIG arc. About three to four times as much wear resistance and hardness as the base material was present on the coated surface. Significant improvements were made to the changed surface's hardness and wear behavior [11]. W. Xinhong et al. created an in-situ technique coating to create TiC particle reinforced Fe-based surface composite by TIG process by depositing a mixture of graphite, ferrotitanium powder, and Fe-based self-fluxing FeCrBSi powder on AISI 1045 steel substrate. The TiC particles, with a size range of 3-5µm, were synthesized from ferrotitanium and graphite powder and evenly distributed. The increased concentration of TiC particles in the matrix enhanced the composite coating's toughness and wear resistance [12]. G. Chen et al. [13] modified the surface of powdered stellite-6 onto SUS403 base using TIG and laser cladding techniques. The substrate, TIG-clad surface, and laser-clad surface have hardness values of 670, 420, and 200 (Hv50), respectively. The substrate,

University of Thi-Qar Journal

ISSN (print): 2706- 6908, ISSN (online): 2706-6894

Vol.19 No.1 Agu. 2024

TIG-clad surface, and laser-clad surface had specific wear rates of 2.3x10-8 mm2/kg, 1.8 x10-8 mm2/kg, and 0.8x10-8 mm^2/kg, respectively. The surface covered with lasers has the maximum hardness and the lowest specific wear rate. Alazzawi et al. deposited AlCrCoFeMnNi high entropy alloy as a coating material on the surface of Ti-6Al-4V alloys to improve its surface properties using TIG welding process. The results showed that the microhardness is significantly improved [14].

TIG arc surfacing is one of the more affordable cladding techniques. It creates a composite layer with a high surface thickness made of intermetallic compounds. The unique benefit of TIG arc surfacing is its ability to form metallurgical bonds [15].

This study emphasize on the using of the Ti6Al4V alloy, gray cast iron, and Fe powders to produce hard facing protection coating to improve the tribological properties of several materials using tungsten inert gas process

2. MATERIALS AND EXPERIMENTAL PROCEDURE

In the this section, we will explain how our experiments were performed and display the instruments and materials used in the research.

2.1 Materials

Three Specimens of structural steel with dimension of 30 x 40 x 6 mm were cut from raw material by saw machine as substrates. The composition of structural steel presented in Table 2. The coated surface must be clean and free of contaminations. Thus, a brush from steel was used to remove the contaminants. Then rinsed with distilled water and acetone to remove the oil traces. To increase the

University of Thi-Qar Journal

ISSN (print): 2706- 6908, ISSN (online): 2706-6894

Vol.19 No.1 Agu. 2024

wettability, the coated surface should be roughed with large size grain emery papers about (120 grit). The cladding material composes of 10 wt.% t of Ti-6Al-4V, 10 wt. % gray cast iron, and 80 wt.% of Fe powders. All of these powders were mixed by mixer for 1 hour the fed to ball mill with milling conditions are :ball to powder ratio (BPR) =10:1, 300 rpm, and milling time 20 hr. After that the milled powders pressed to form rectangular flakes with 10x 30x 3mm dimensions. The flakes then placed upon the surface of substrate. TIG welding machine used to melt on the substrate. Table 1 presents the TIG cladding process parameters that used in this study. Table 1 shows the cladding parameter that used in the current study. Vickers CV-400DM micro-hardness tester was used to measure the hardness of the weld joint at loading of 200 gram and hold for 15 seconds. At least five point on the surface of the surface of cladding layer were investigated to determine the surface hardness. Shimadzu XRD-6000 diffractometer analysis will be used for identifying the constituent phases. The Cu- Kα anode diffract meter with Θ-2Θ goniometer is appropriate to conduct the analysis. The scanning range is 20^{o}– 90^{o}, with scanning speed 0.2^{o} degrees per minute**.** A falex-ISC200 Pin on disk wear test machine was used to evaluate the wear resistance of the as deposited cladded layer on the carbon steel. XJD-100-monocolor optical microscope was employed to capture worn surfaces images. OriginLab was used to plot hardness curves. To determine the weight losses, Sartorius high precision 4 digits balance was used. The wear conditions that adopted in this study are 400 rpm represents the disc speed, 75mm is the diameter of wear track, and 5 min is the sliding distance. The counter disk was from HSS with 120 mm diameter and 4 mm thickness. Wear samples were cut from the cladding sample as pin with dimensions (5mm diameter and 15mm length).

University of Thi-Qar Journal

ISSN (print): 2706- 6908, ISSN (online): 2706-6894

Vol.19 No.1 Agu. 2024

Table 1. Shows the process parameters

Parameters	Levels
Cladding currents (Amp)	90
Gas flow rate (l/min)	9 – 10- 11
Welding voltage	Constant
Scanning speed (mm/s)	1.3
Arc length (mm)	3 to 4
Powder thickness (mm)	2 to 2.5
Electrode tip angle	30 degree
Torch angle	90 degree

Table 2. chemical composition of structural steel [16]

C	Si	Mg	Cu	P	Cr	Ni	Sn	Fe
0.18	0.23	0.8	0.2	0.03	0.04	0.05	0.0	balance

3. RESULTS AND DISCUSSIONS

In this section, our results will be interpreted and analyzed, discussions will be introduced to correlate the outcomes.

3.1. Surface morphology

Figure 1 presents the surface topography of the cladding tracks that prepared under different flow rates of shielding gas and constant welding current and welding speed using TIG welding process. The

University of Thi-Qar Journal

ISSN (print): 2706- 6908, ISSN (online): 2706-6894

Vol.19 No.1 Agu. 2024

cladding tracks show good quality with low rippling marks and splash. Also, there is no under cuts and cracks and uniform thickness with good reflectively, excellent reinforcement and no porosity.

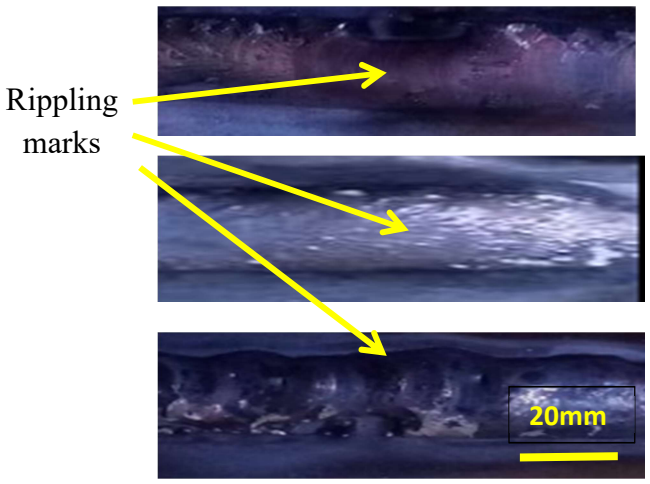

Fig.1. cladding pass of the TIG cladding layers.

3.2. Microstructure characterization

Figure 2 shows the microstructures of the top zone of the samples that fabricated under different gas flow rates and constant current and scanning speeds. From this figure, it can be seen that the structure of all samples at this point revealed a brightness and darkness area the brightness represents the main dendrite (DR), which consists of the high melting point while the brightness regions indicate to the inner dendrite that usually include the low melting point metallic elements. The microstructures also be showed the precipitates of an expected carbides and intermetallic compounds that associated with chemical interactions between defused free carbons which decomposed from the cementite and graphite and the constituent elements of the grade 5 alloys and cast iron alloy from one side and the Fe-atoms on the other side. The effect of the argon shielding flow rate seems clear when comparing the grain size of these sample. Where the sample that fabricated at low flow rate showed the larger grain size structure than the

University of Thi-Qar Journal

ISSN (print): 2706- 6908, ISSN (online): 2706-6894

Vol.19 No.1 Agu. 2024

others. These structures can be attributed into the difference in cooling rates. Figure 3 shows the microstructure along the transvers cross section. Where there are four zones can be distinguished in the cross section are: base metal zone (BMZ), heat effected zone (HZ), bonding zone (BZ) , and cladding zone (CZ). Curved shape of bonding line indicates that the cladding layers have excellent bond with base material. From Figure 3 a, it can be seen that the cladding layer zone exhibit equated grains with fine dispersion solid TiC particles. Figure 3 b represents the bonding zone its consists of planner growth indicates to the interface and columnar grains directed toward the center of the cladding pool and shrinkage cavities. Figure 3 c shows the microstructure of the HAZ zone, due to the high temperature that this zone is exposed to, it induces coarse-grained microscopic structure with ferrite deposition along the grain boundaries. Tables 2 and 3 shows the chemical composition of the Ti-6Al-4V alloy and the cast iron alloy. The chemical composition of the alloys was done using XRF analyzer in the material lab of the Nasiriyah power plant.

University of Thi-Qar Journal

ISSN (print): 2706- 6908, ISSN (online): 2706-6894

Vol.19 No.1 Agu. 2024

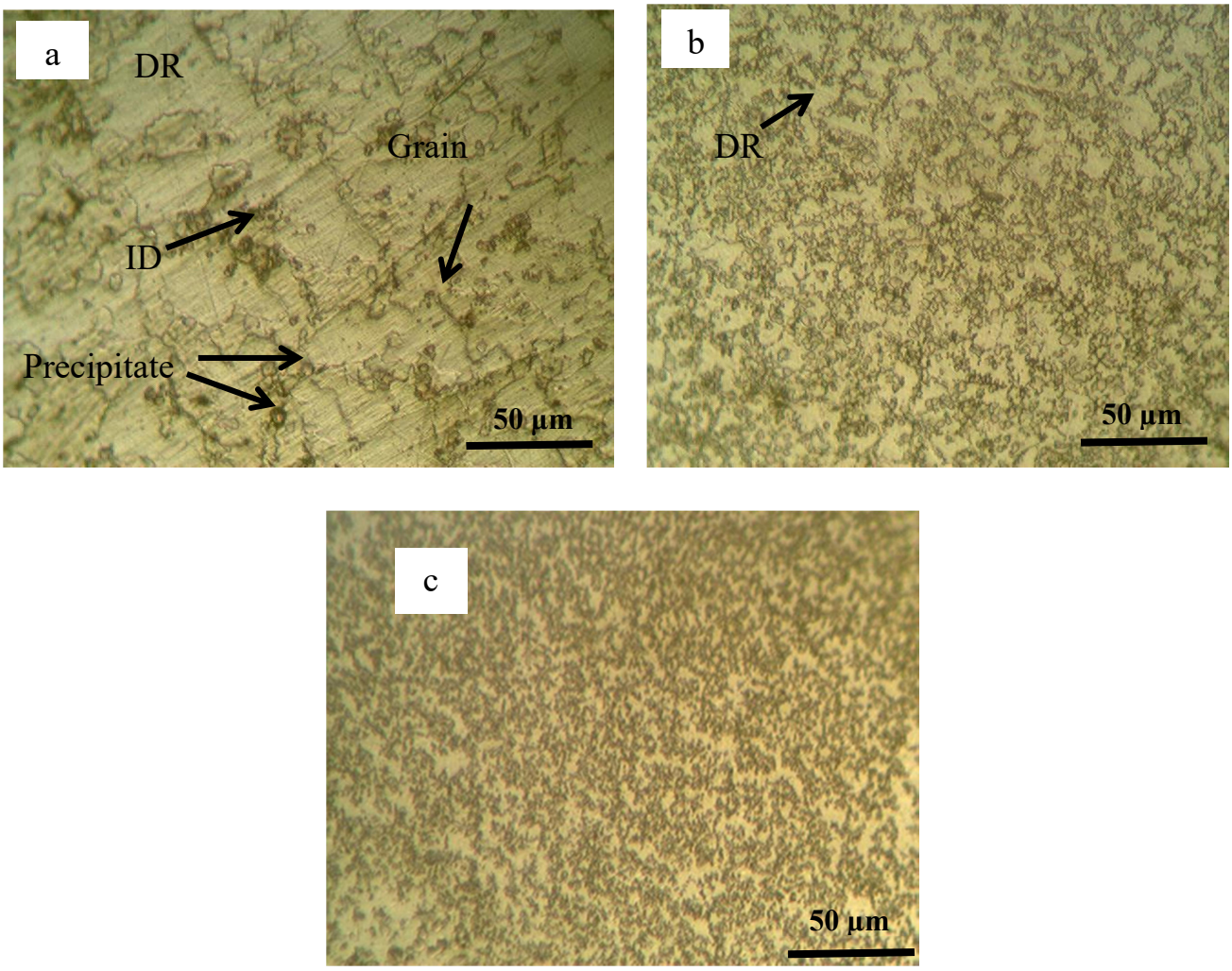

Fig. 2. The microstructures of the samples that prepared under different gas flow rates: (a) 9 l/min, (b) 10 l/min, (c) 11 l/min.

University of Thi-Qar Journal

ISSN (print): 2706- 6908, ISSN (online): 2706-6894

Vol.19 No.1 Agu. 2024

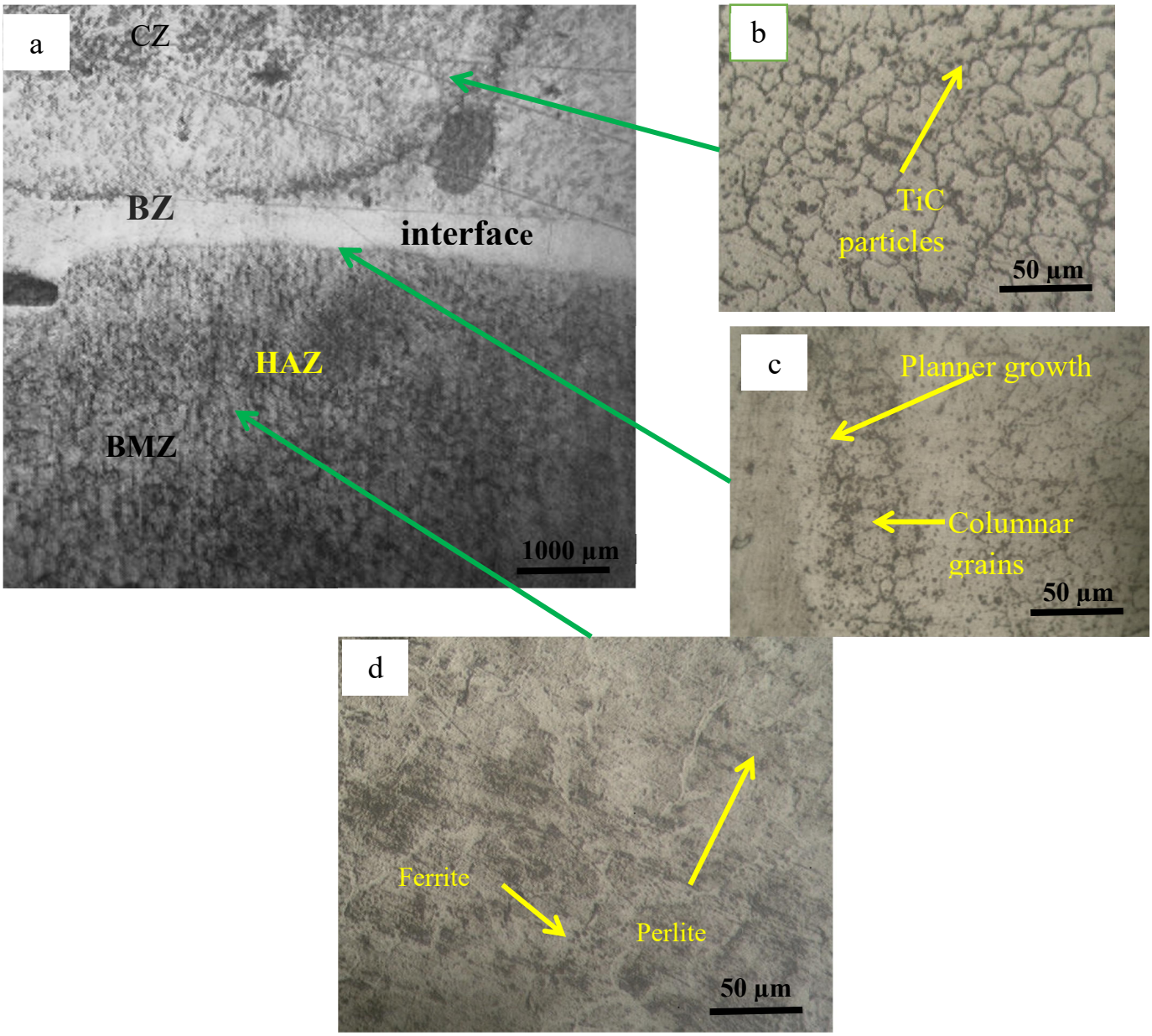

Fig.3. (a)The microstructure zones along the transverse cross-section, (b) cladding zone, (c) bonding zone, and (d)base metal and HAZ zones.

University of Thi-Qar Journal

ISSN (print): 2706- 6908, ISSN (online): 2706-6894

Vol.19 No.1 Agu. 2024

Table 3. Chemical contents of Ti6Al4V alloy.

Element	*Content in %*	*XRF result %*
	Ref.	*Nom.*
Aluminum (Al)	5.5 -6.8	5.65
Vanadium (V)	3.5 - 4.5	3.72
Carbon (C)	0.1	-------
Iron (Fe)	0.3	3.2
Oxygen (O)	0.2	-------
Nitrogen (N)	0.05	------
Titanium (Ti)	Balance/ Base	86

3.3. Characterization of the Phase Composition

Figure 4 represents the x-ray diffraction peaks of the Ti-6Al-4V alloy chips. This figure illustrate that the Ti6Al4V alloy composes of, α-Ti phase which is indicated by (100), (101), (102), (110), (112), (201) and (104) planes, and a small amount of β-Ti phase represented by (110) and (211). For indexing the planes both the origin lab and Xpert high score softwares were used to determine the Miller indices, and these results were checked with Brag and lattice spacing calculations. Figures 5 shows the x-ray patterns of the three samples that prepared at different flow rate of shielding gas. Brags law and lattice distance spacing formulas were used to index the present phases. The results refer that the cladding layers are composed of body centric cubic (BCC) and face centric (FCC) and traces that can be suggested to be TiC, TiSi, and Fe3C. The BCC phase is considered to the dominant phase and it's percentage increases with increasing the cooling rate.

University of Thi-Qar Journal

ISSN (print): 2706- 6908, ISSN (online): 2706-6894

Vol.19 No.1 Agu. 2024

$$2d \sin\theta = n\lambda \dots\dots\dots\dots\dots\dots\dots 3.1 \quad [17]$$

$$d = \frac{a}{\sqrt{h^2+k^2+l^2}} \dots\dots\dots\dots\dots 3.2 \quad [17]$$

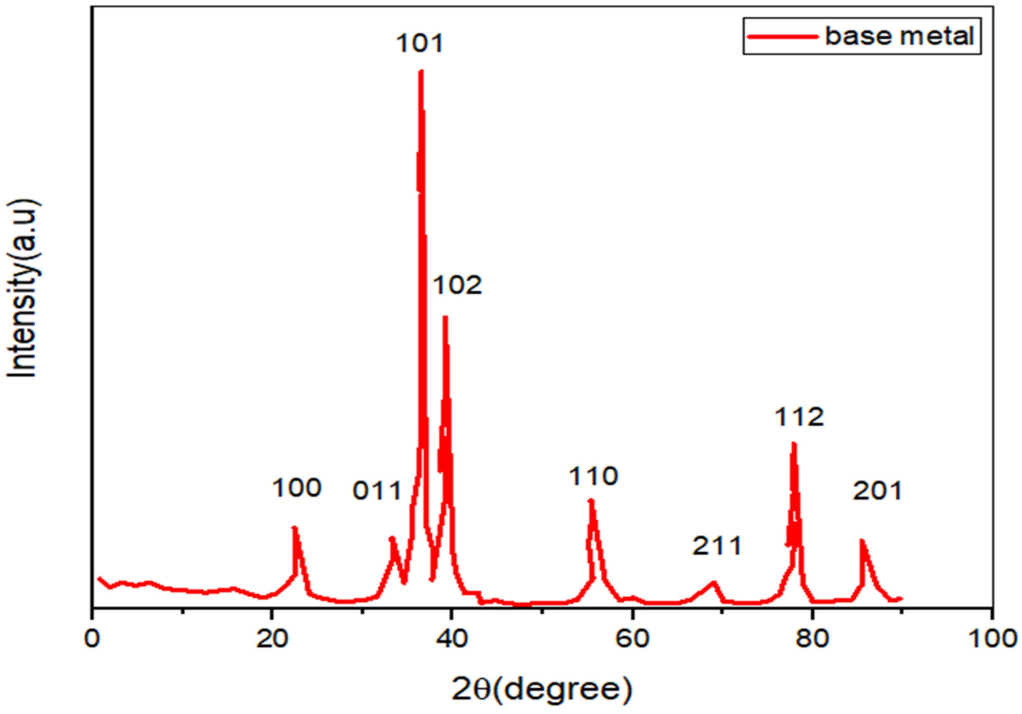

Fig.4. XRD pattern of the Ti6Al4V alloy.

University of Thi-Qar Journal

ISSN (print): 2706- 6908, ISSN (online): 2706-6894

Vol.19 No.1 Agu. 2024

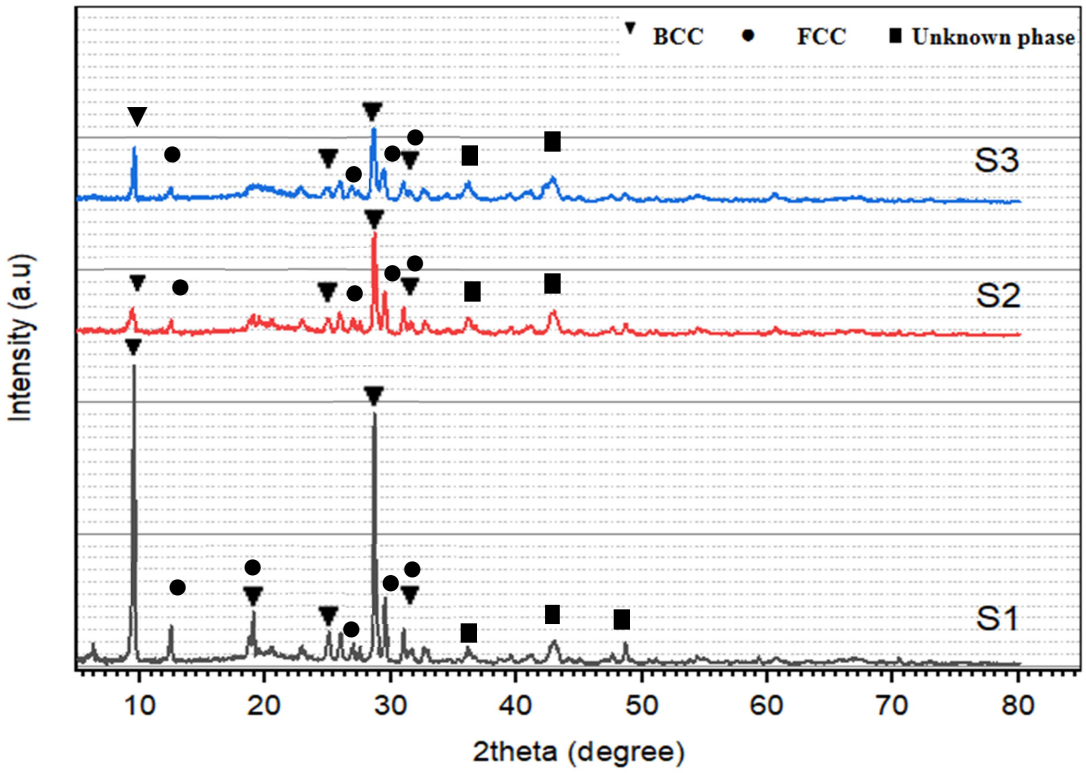

Fig.5. XRD pattern of samples 1, 2 and 3 at different gas flow rate (l/min).

3.4. Micro-hardness Characterization

High cooling rate due to an increase in the gas flow leads to form very fine dendrite as shown in Figure 3 and increase in the BCC formation also increases in the amount of the cementite (Fe3C) and titanium carbide (TiC) in hard facing layers . Titanium carbide is formed due the interaction between the titanium and free carbon which realized from cementite or graphite in the iron alloy by decomposition of these components. Titanium has high affinity with free carbon. This can be confirmed with what was obtained in the literature when comparing the peaks of XRD characterization. Where the traces of the TiC are found at angular distance 35 to 36 and Fe3C

University of Thi-Qar Journal

ISSN (print): 2706- 6908, ISSN (online): 2706-6894

Vol.19 No.1 Agu. 2024

traces between 40 to 45 degree with small peak intensity when reducing the significant peaks value of the X'Pert HighScore software these traces and distance degree met with what was reported by Cho et al. [18]. High cooling rate leads to increase these the sharpness of their peaks in the cladding layers which in turn increase the micro-hardness. The average micro-hardness of layers is about three times more than that the base metal. Figure 6 shows the micro-hardness profile of three samples.

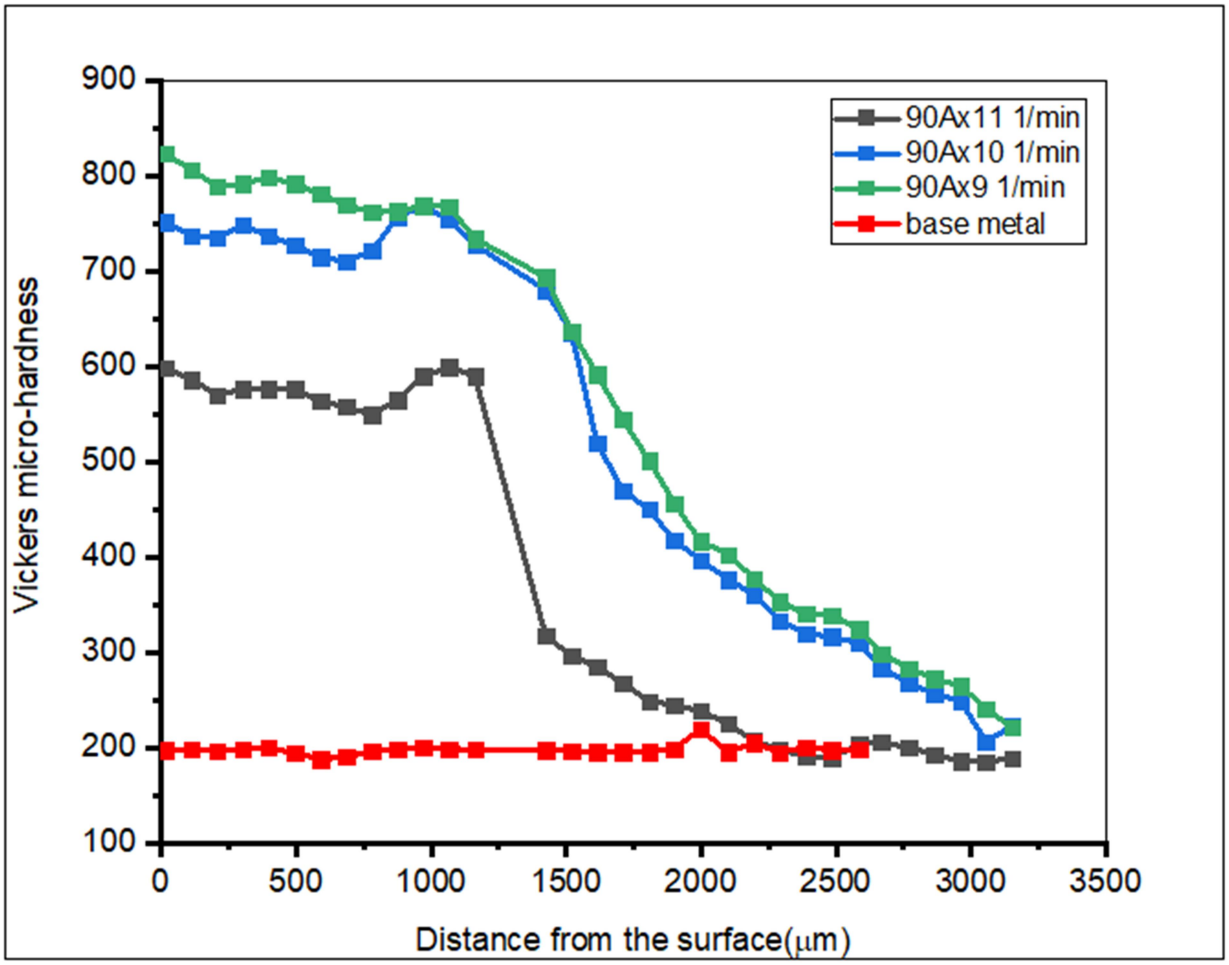

Fig.6. Micro-hardness profiles of the TIG coating samples at different gas flow rates.

University of Thi-Qar Journal

ISSN (print): 2706- 6908, ISSN (online): 2706-6894

Vol.19 No.1 Agu. 2024

3.5. Wear analysis

The wear value in terms of weight loss of the cladding pins was carried out at different vertical load for the samples that fabricated under different gas flow rate and constant current. These pins were cut from cladding samples with dimensions (5x5x10) mm. Pins were tested at 1 Kg normal load, 200s-rpm speed of disc, 16 mm sliding radius at room temperature, and 10 min sliding time. The counter abrasive part is made of the high-speed steel HSS with outer diameter 120-mm. high prescient balance with 0.1 mg accuracy was used to measure the weight losses. Both rubbing surfaces were grounded using 1000 grade SiC paper to obtain roughness less than 4 micron. According the Archard equation (Eq.3.3) the wear rate is inversely proportion with hardness. Where the layer that has high surface micro hardness exhibited lower wear rate. Equation 3.4 was used to evaluate the wear rate of three cases. Figure 7 illustrates the friction coefficient profiles. From this figure, it can be seen that the wear resistance of the low carbon steel has been improved when depositing the proposed coating materials. Table 4 shows the coefficient of friction and wear rate of three layers. Where the cladding layers that prepared at high flow rates reveal wear rate about two times than that of the substrate. Figure 8 shows the optical images of the worn surfaces of the cladding layers. It can be seen that the worn surfaces exhibit abrasive wear mode for samples 2 and 3 and adhesive because they have high micro-hardness, while sample 1 reveals adhesive/abrasive modes.

$$Q = \frac{KWL}{H} \dots\dots\dots\dots\dots\dots .3.3 \text{ [19]}$$

University of Thi-Qar Journal

ISSN (print): 2706- 6908, ISSN (online): 2706-6894

Vol.19 No.1 Agu. 2024

Q: represents volume of wear debris, K: constant, w: normal load, L: sliding distance, and H: surface hardness.

$$WR = \frac{\Delta W}{2\pi rn} \quad \ldots\ldots\ldots\ldots\ldots\ldots 3.4 \text{ [19]}$$

ΔW: Weight loss (g) .

r: The radius of the sample (15mm).

n: Disk rotational speed (rpm).

t: Sliding time (min.).

Table 4. Shows the COF and wear rate of layers

	Base metal	**S 1**	**S 2**	**S 3**
Friction coefficient (Max.)	1.1806	0.7646	0.7441	0.6082
Friction coefficient (Av)	0.9447	0.698	0.4613	0.5922
Wear rate (g/m)	9.288×10^{-7}	7.6433×10^{-7}	6.369×10^{-7}	5.552×10^{-7}

University of Thi-Qar Journal

ISSN (print): 2706- 6908, ISSN (online): 2706-6894

Vol.19 No.1 Agu. 2024

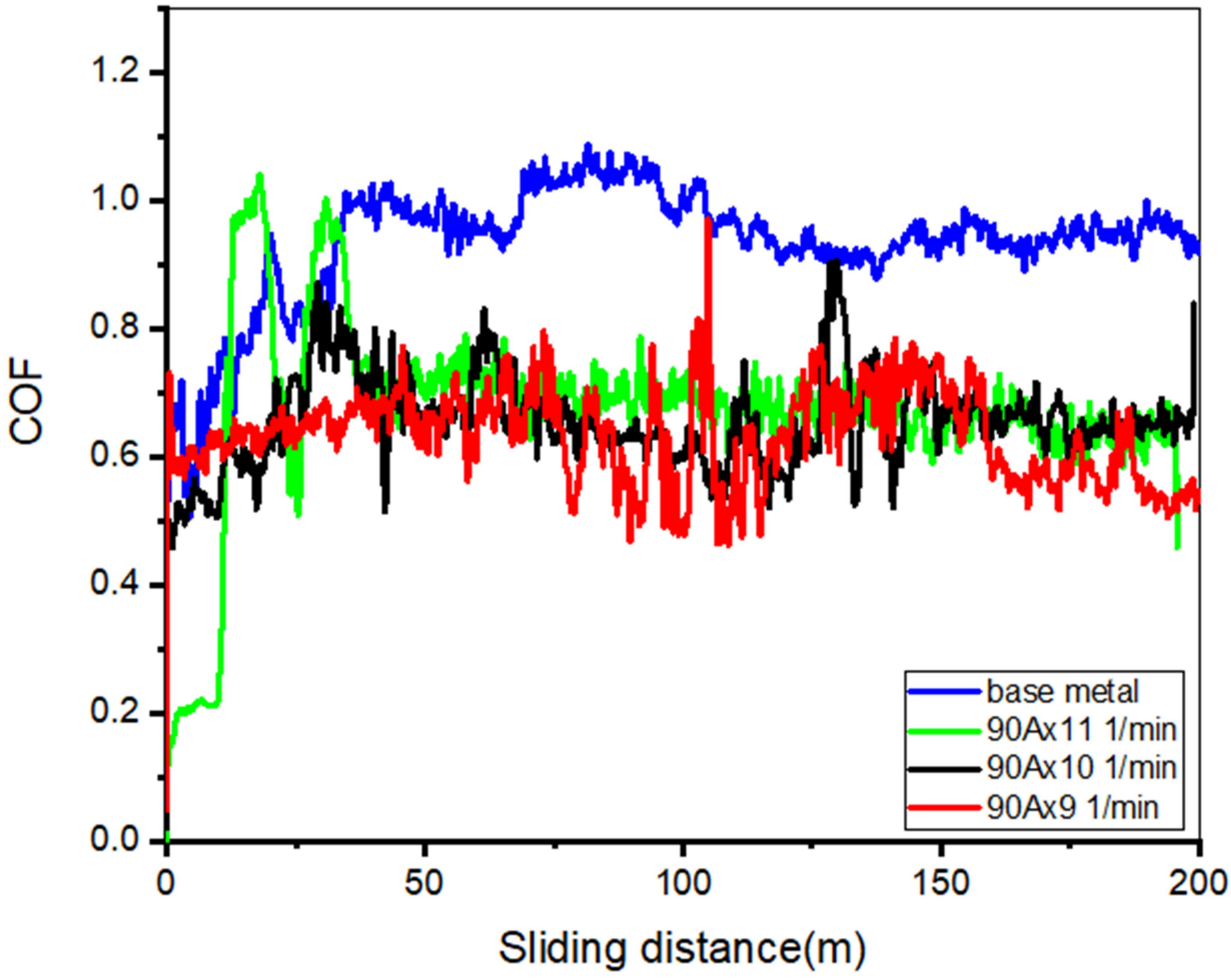

Fig. 7. .Friction coefficient as a function of the sliding distance of the cladding layers.

University of Thi-Qar Journal

ISSN (print): 2706- 6908, ISSN (online): 2706-6894

Vol.19 No.1 Agu. 2024

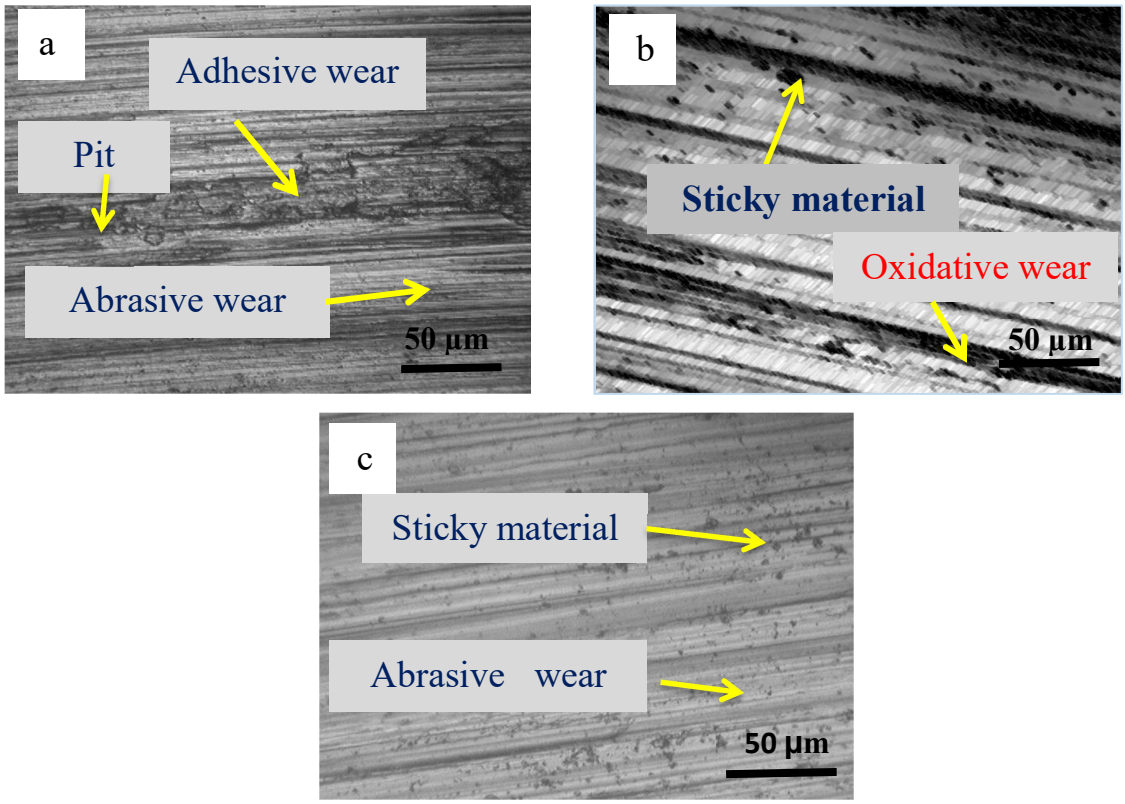

Fig. 8. Optical images of the worn surfaces (a) sample1, (b) sample 2, and (c) sample 3.

4. CONCLUSIONS

From the results, many conclusions can be drawn. It can be cladded the low carbon steel with preplaced powder consists of 10% iron, 10% Ti-6Al-4V, and 80% Fe as a preplaced hard facing coating materials using TIG welding process. Microstructure examination reveals that the cladding layers are composed of dendrite and inter dendrite and size of this structure is changed when increasing the gas flow rate. Moreover, XRD investigation shows that the cladding layers include FCC and BCC phases with small amount of unknown phase and the dominant phase is the BCC. Micro-hardness evaluation of the cladding layers reveals that the cladding layers which produced

under high range of shielding gas flow rates have high surface hardness. Friction coefficient and wear rate of the substrate are improved by 2 times and 1.5 times, respectively especially with increasing the gas flow rate.

REFERENCES:

[1] C.-W. Kim, H.-S. Yoo, J.-Y. Jeon, K.-T. Cho, and S.-W. Choi, "Study on Improvement of Surface Properties of Low Carbon Steel Using Laser Cladding," *Archives of Metallurgy and Materials,* pp. 1033-1036, 2021, doi: 10.24425/amm.2021.136420.

[2] S. Swirad, A. Gradzik, K. Ochal, and P. Pawlus, "Effects of the surface layer of steel samples after ball burnishing on friction and wear in dry reciprocating sliding," *Sci Rep,* vol. 13, no. 1, p. 11315, Jul 13 2023, doi: 10.1038/s41598-023-38534-7.

[3] R. N. Elshaer, S. El-Hadad, and A. Nofal, "Influence of heat treatment processes on microstructure evolution, tensile and tribological properties of Ti6Al4V alloy," *Sci Rep,* vol. 13, no. 1, p. 11292, Jul 12 2023, doi: 10.1038/s41598-023-38250-2.

[4] K. Kumar, C. Sateesh Kumar, M. Masanta, and S. Pradhan, "A review on TIG welding technology variants and its effect on weld geometry," *Materials Today: Proceedings,* vol. 50, pp. 999-1004, 2022, doi: 10.1016/j.matpr.2021.07.308.

[5] R. Bianco and R. A. Rapp, "Pack cementation diffusion coatings," in *Metallurgical and Ceramic Protective Coatings*, K. H. Stern Ed. Dordrecht: Springer Netherlands, 1996, pp. 236-260.

[6] A. Hallén and M. Linnarsson, "Ion implantation technology for silicon carbide," *Surface and Coatings Technology,* vol. 306, pp. 190-193, 2016, doi: 10.1016/j.surfcoat.2016.05.075.

[7] A. Dan, P. K. Bijalwan, A. S. Pathak, and A. N. Bhagat, "A review on physical vapor deposition-based metallic coatings on steel as an alternative to conventional galvanized coatings," *Journal of Coatings Technology and Research,* vol. 19, no. 2, pp. 403-438, 2022/03/01 2022, doi: 10.1007/s11998-021-00564-z.

[8] B. Zohuri, "Laser Surface Processing," in *Thermal Effects of High Power Laser Energy on Materials*, B. Zohuri Ed. Cham: Springer International Publishing, 2021, pp. 331-362.

[9] F. Babadjanov, U. Specht, T. Lukasczyk, and B. Mayer, "Heat Accumulation-Induced Surface Structures at High Degrees of Laser Pulse Overlap on Ti6Al4V Surfaces by Femtosecond Laser Texturing," *Materials (Basel),* vol. 16, no. 6, Mar 21 2023, doi: 10.3390/ma16062498.

[10] S. Islak, D. Kır, and S. Buytoz, "Effect of sintering temperature on electrical and microstructure properties of hot pressed Cu-TiC composites," *Science of Sintering,* vol. 46, no. 1, pp. 15-21, 2014, doi: 10.2298/sos1401015i.

[11] K. Cooke and A. Alhubaida, "Microstructural response and wear behaviour of Ti-6Al-4V impregnated with Ni/Al(2)O(3) + TiO(2) nanostructured coating using an electric arc," *Sci Rep,* vol. 12, no. 1, p. 21978, Dec 20 2022, doi: 10.1038/s41598-022-25918-4.

[12] W. Xinhong, Z. Zengda, S. Sili, and Q. Shiyao, "Microstructure and wear properties of in situ TiC/FeCrBSi composite coating prepared by gas tungsten arc welding," *Wear,* vol. 260, no. 7, pp. 705-710, 2006/04/07/ 2006, doi: https://doi.org/10.1016/j.wear.2005.03.018.

[13] C. Chen, W. Meiping, H. Rui, G. Yuling, and M. Xiaojin, "Understanding Stellite-6 coating prepared by laser cladding: Convection and columnar-to-equiaxed transition," *Optics & Laser Technology,* vol. 149, p. 107885, 2022/05/01/ 2022, doi: https://doi.org/10.1016/j.optlastec.2022.107885.

[14] F. Alazzawi, H. Aghajani, and A. Kianvash, "Surface Improvement of Ti-6Al-4V Alloy by Deposition of AlCrCoFeMnNi High Entropy Alloy Using TIG Process," *JOM,* vol. 76, no. 2, pp. 656-666, 2024/02/01 2024, doi: 10.1007/s11837-023-06314-3.

[15] S. R. Singh and P. Khanna, "A-TIG (activated flux tungsten inert gas) welding: – A review," *Materials Today: Proceedings,* vol. 44, pp. 808-820, 2021, doi: 10.1016/j.matpr.2020.10.712.

[16] A. Rajput and J. K. Paik, "Effects of naturally-progressed corrosion on the chemical and mechanical properties of structural steels," *Structures,* vol. 29, pp. 2120-2138, 2021/02/01/ 2021, doi: https://doi.org/10.1016/j.istruc.2020.06.014.

[17] D. D. Le Pevelen, "Small Molecule X-Ray Crystallography, Theory and Workflow," in *Encyclopedia of Spectroscopy and Spectrometry (Second Edition)*, J. C. Lindon Ed. Oxford: Academic Press, 2010, pp. 2559-2576.

[18] S. Cho *et al.*, "Enhancing high-temperature properties of stainless steel composite with titanium carbide reinforcement: a study on coefficient of thermal expansion, thermal conductivity, and strength," *Journal of Materials Research and Technology,* vol. 25, pp. 7241-7253, 2023, doi: 10.1016/j.jmrt.2023.07.162.

[19] L. Frérot, R. Aghababaei, and J.-F. Molinari, "A mechanistic understanding of the wear coefficient: From single to multiple asperities contact," *Journal of the Mechanics and Physics of Solids,* vol. 114, pp. 172-184, 2018/05/01/ 2018, doi: https://doi.org/10.1016/j.jmps.2018.02.015.